ACSNANO

www.acsnano.org

ARTICLE

Intermolecular Forces Dictate Vibrational Energy Transfer in Plasmonic–Molecule Systems

Ziwei Yu and Renee R. Frontiera*

Cite This: *ACS Nano* 2022, 16, 847–854

Read Online

ACCESS | Metrics & More | Article Recommendations | Supporting Information

ABSTRACT: Plasmonic materials are a promising category of photocatalysts for solar energy harvesting and conversion. However, there are some significant obstacles that need to be overcome to make plasmonic catalysts commercially available. One major challenge is to obtain a systematic understanding of how to design and optimize plasmonic systems from the perspective of both plasmonic materials and reagent molecules to achieve highly efficient and selective catalysis. It is well-known that the contributions of plasmon–molecule interactions such as plasmon-induced resonant energy transfer and charge transfer to the catalytic mechanism are rather complicated and possibly multifold. Observation of these phenomena is challenging due to the highly heterogeneous nature of plasmonic substrates as well as the large difference in sizes and optical cross sections between plasmonic materials and molecules. In this work, we use a molecular perspective to examine the crucial process of energy transfer between plasmons and molecules, with the goal of determining which experimental parameters can be used to control this energy flow. We employ ultrafast surface-enhanced anti-Stokes and Stokes Raman spectroscopy to investigate vibrational energy transfer in plasmonic–molecule systems. By comparing the energy transfer kinetics of five different aromatic thiols on the picosecond time scale, we find that intermolecular forces play an important role in energy distribution in molecules adsorbed to plasmonic materials, which changes the amount of energy deposited onto the molecule and the lifetime of the energy deposited. Our work implies that careful consideration of catalyst loading and molecule adsorption geometry is crucial for enhancing or suppressing the rate and efficiency of plasmon-driven energy transfer.

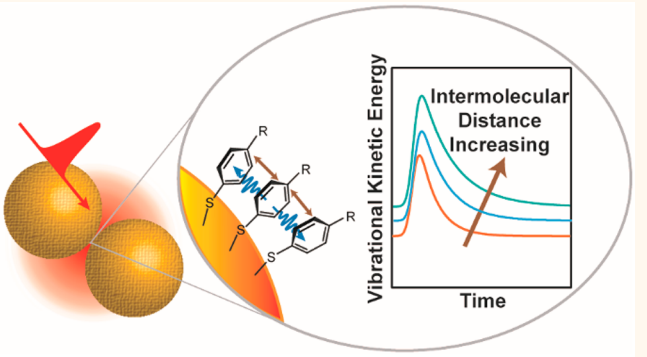

KEYWORDS: *plasmonic photocatalysis, ultrafast surface-enhanced Raman spectroscopy, plasmon-driven energy transfer, intermolecular interactions, intermolecular energy transfer*

Utilization of green energy is an important aspect of the worldwide efforts toward sustainable development, and solar energy harvesting is one of the most promising fronts. Using sunlight to drive chemical reactions creates the possibility of largely cutting down energy consumption in the chemical industry and thus inspires the development of a range of photocatalysts.[1−6] Plasmonic materials, an emerging class of photocatalysts, are metal or metal-like nanomaterials that can concentrate light down to nanoscale volumes through excitation of a localized surface plasmon resonance (LSPR). LSPR is a collective oscillation of electrons at the interface of a plasmonic material and a dielectric and is excited by resonant light.[7] Shortly after excitation, the LSPR loses coherence and partitions its energy through the formation of energetic electrons/holes, hot lattice, and heated environment.[8,9] This nanoscale light confinement and decay processes create energy-rich conditions where a range of chemical reactions can occur. For instance, industrially relevant yet energy-consuming chemical reactions such as water splitting,[10] CO_2 reduction,[11] and ammonia synthesis[12] have been demonstrated with plasmonic catalysts at ambient conditions. In addition to the advantages of a light-driven catalytic process, high selectivity is also observed with many plasmon-driven reactions including methyl migration,[13] amine

Received: September 24, 2021
Accepted: December 17, 2021
Published: December 22, 2021

https://doi.org/10.1021/acsnano.1c08431
ACS Nano 2022, 16, 847–854

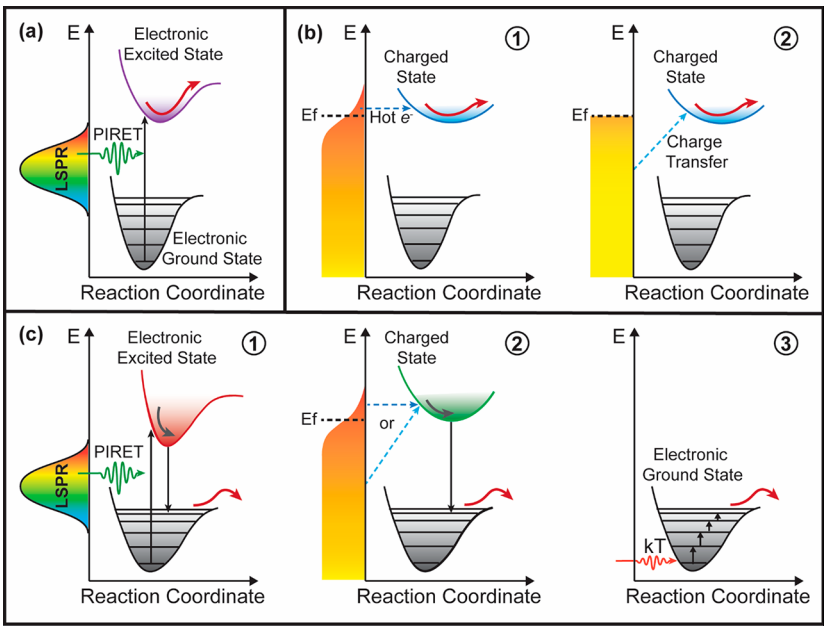

Figure 1. Plasmon-induced chemical transformation initiated from (a) electronically excited state through resonant energy transfer, (b) charged state through indirect (b1) and direct (b2) charge transfer, and (c) vibrationally excited state through relaxation from electronically excited state (c1), transient charge transfer (c2), and heating (c3).

oxidation,[14] aromatic alcohol oxidation,[15,16] and CO_2 hydrogenation.[11] Moreover, the LSPRs of plasmonic materials are easily tunable over the visible spectrum by changing their size, shape, or composition, which adds another strength to plasmonic catalysts for sunlight harvest over their semiconductor conterparts.[17−20]

However, since their discovery, plasmonic photocatalysts have not yet been widely adopted or commercialized in industrial applications. One challenge is that the quantum efficiency is generally too low and the cost of the substrate is too high to displace existing technologies. For example, the external quantum efficiency of water splitting on a gold nanorod array was reported to be <1% by Mubeen and coworkers.[21] Another challenge is the lack of design principles for plasmonic catalysis for chemical synthesis of specific products, which usually requires prediction and control over complicated chemical transformations. To obtain better guidelines for plasmonic catalyst design and optimization from the perspective of both the plasmonic materials (morphology, composition, ...) and molecules (starting reagents, adsorption geometry, pretreatment conditions, ...), a fundamental understanding of plasmon catalytic mechanism is crucial. In plasmonic−molecule systems, multiple LSPR energy partitioning processes such as resonant energy transfer, charge transfer, and localized heating could happen before and as the LSPR decays and potentially contribute to the reactivity. Significant prior research has been trying to resolve the complicated and possibly multifold plasmon−molecule interactions, but no consensus has been reached yet due to the limitation of current techniques and the complicated nature of those interactions which are highly dependent on the physical and chemical properties of both the plasmonic materials and the molecules. However, by considering plasmon catalysis from the molecular point of view, we are able to quantify energy transfer processes in plasmonic−molecule systems that will ultimately undergo reactions.

Here we classify three different molecular-oriented pathways relevant to the reaction dynamics in a plasmonic catalytic system, as depicted in Figure 1: molecular transformation initiating from the (i) excited electronic state, (ii) charged state, or (iii) vibrationally excited ground electronic state. In the first scenario (Figure 1a), when there is an overlap between the plasmon energy and the molecule electronic transition energy, plasmon energy is resonantly transferred to adjacent molecules before the plasmon decoheres, preparing the molecules in the electronic excited state, which can lead to chemical transformation.[22] In the second scenario, a charged state is formed through indirect or direct electron/hole transfer from the metal to molecules (Figure 1b). In the case of indirect charge transfer (Figure 1b1), hot electrons and holes are formed in the metal as a result of LSPR decay and can transfer to unoccupied molecular orbitals when the energy levels are aligned.[23] For direct charge transfer (Figure 1b2), electrons/holes are transferred directly from the metal to the adsorbed molecules when the transition energy is on resonance with the plasmon energy.[24] In both cases, a main characteristic of charge transfer is the shift in molecular vibrational frequencies because of the change in nuclear geometry, and both pathways prepare the molecules in the charged state as the reaction intermediate. In the third scenario, molecules at ground electronic state can overcome the energy barrier to chemical reactions when vibrationally excited (Figure 1c). Molecules gain vibrational energy through multiple pathways, including relaxation from electronic excited states (Figure 1c1), transient charge transfer (Figure 1c2), lattice energy transfer, and heat conduction (Figure 1c3).[24] Although there could still be electronic transition or charge transfer involved, the main difference is that the electronic excited state or charged state is short-lived so the chemical transformation happens with molecules at the electronic ground state.

Investigating the plasmon catalytic mechanism from a molecular picture gives important information related to the efficiency and selectivity of chemical reactions. In this study,

https://doi.org/10.1021/acsnano.1c08431
ACS Nano 2022, 16, 847−854

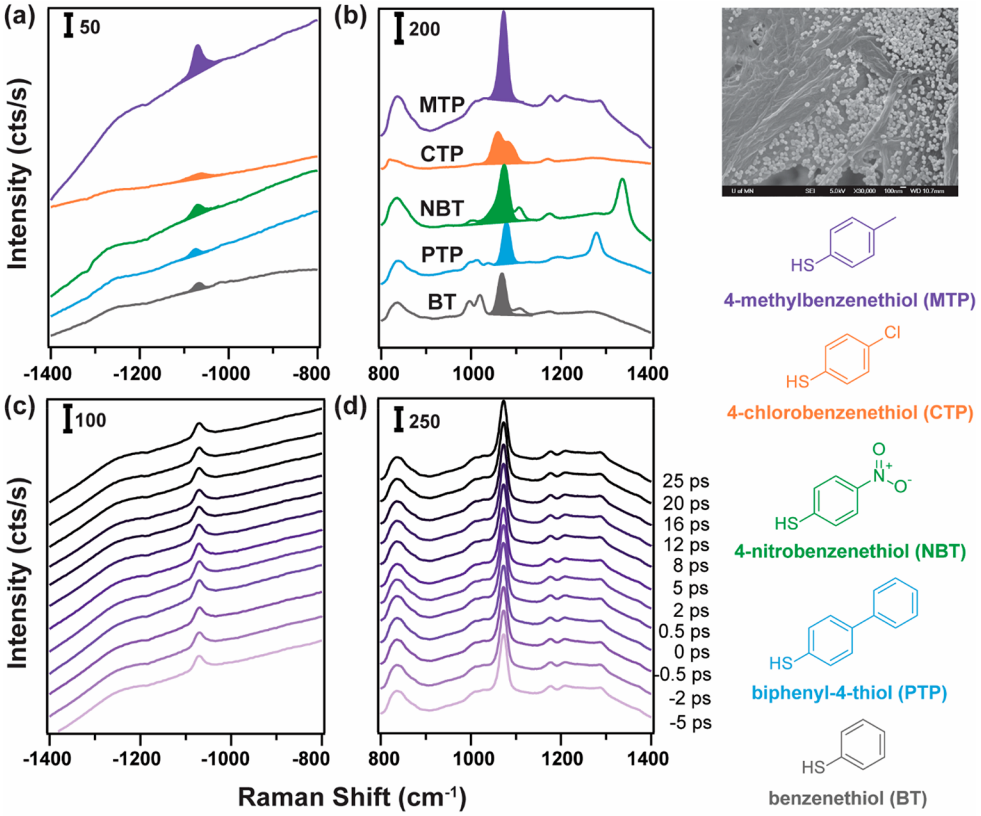

Figure 2. (a) Anti-Stokes and (b) Stokes spectra of 4-methylbenzenethiol (MTP, purple), 4-chlorobenzenethiol (CTP, orange), 4-nitrobenzenethiol (NBT, green), biphenyl-4-thiol (PTP, blue), and benzenethiol (BT, gray) at time zero with a 50 W/cm^2 pump pulse and a 300 W/cm^2 probe pulse. Transient (c) anti-Stokes and (d) Stokes spectra of MTP with a 50 W/cm^2 pump pulse and a 300 W/cm^2 probe pulse. Inset picture on the upper left shows the SEM image of the plasmonic substrate.

we are particularly interested in the third pathway as described above, where molecules gain sufficient vibrational energy to overcome chemical reaction barriers. For this pathway, the lifetime of the vibrational energy and the mode specificity of energy transfer are of particular interest. First of all, a longer lifetime of the vibrationally pumped molecular state means a greater chance for the chemical transformation to happen. Moreover, localization of the vibrational energy on certain molecular coordinates controls the direction of the chemical reactions.[25] Therefore, an understanding of the plasmon catalytic mechanism from the molecular point of view could provide insights toward possible approaches to control and localize vibrational energy onto desired reaction coordinates, which could then contribute to the guidelines for the design and optimization of highly efficient and selective plasmonic catalysts.

RESULTS AND DISCUSSION

To quantitatively monitor molecular vibrational energy with plasmon excitation, our group uses ultrafast anti-Stokes and Stokes surface-enhanced Raman spectroscopy (SERS). A major difficulty of investigating molecular energy in plasmonic systems is to acquire nanoscale information from ensemble measurements on heterogeneous samples. However, SERS is inherently molecule specific and preferentially provides signal from the most active regions of the plasmonic substrates. According to a previous study, 85% of SERS signal comes from 6% of the molecules, which are in the "hottest" hotspots.[26] Consequently, SERS is selectively probing molecules in the hotspots where chemical reactions are most likely to happen. With an ultrafast pump−probe implementation of SERS, we are able to investigate molecular energy deposition on picosecond time scale. Although not sufficient to resolve resonant energy or charge transfer processes, picosecond resolution enables us to track molecular energy on the time scale comparable to molecule structure rearrangement. Therefore, with the motivation of exploring what molecular properties could be tuned to control the vibrational energy transfer from plasmonic materials to adsorbate molecules, we chose a series of aromatic thiols with different substituent groups as probe molecules. Aromatic thiols are known for their ability to form self-assembled monolayers (SAM) on metal surfaces, which ensures the surface selectivity of the SERS measurements.[27−29] They are also sulfur-containing precursors for production of pharmaceutical products and synthesis of thiosugars and thioglycosides.[30−32] However, we should point out that throughout the measurements, the studied molecules are not undergoing chemical reactions with the experimental conditions. This is to avoid the complexity brought by reactivity, which will change the distribution of probed molecules in the hot spots. Herein this study aims to provide some fundamental perspective toward the correlation between molecular properties and plasmon-induced vibrational energy increase, which will lead to valuable insight toward guidelines for plasmon-catalyzed reaction design from a molecular perspective.

An important factor we consider for the ultrafast measurements is the sample stability under the high laser flux. It is well-

https://doi.org/10.1021/acsnano.1c08431
ACS Nano 2022, 16, 847−854

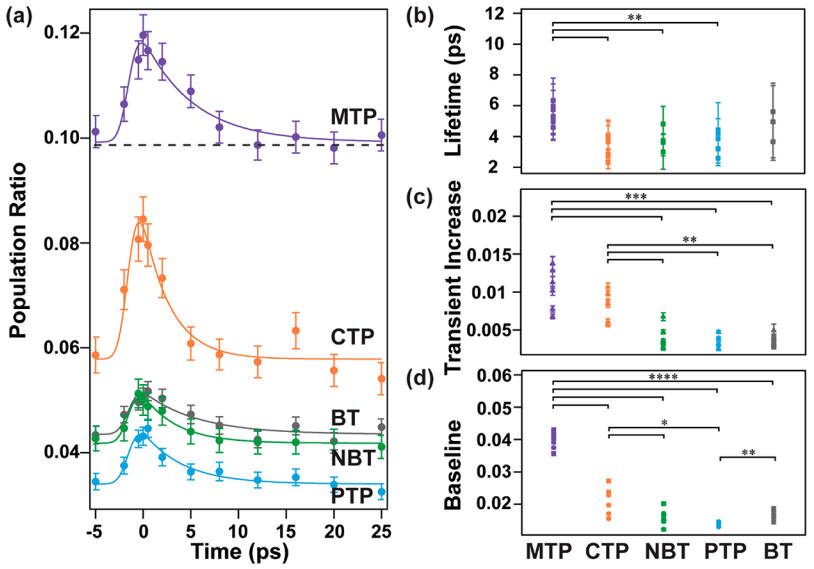

Figure 3. (a) Transient kinetic trace of the excited/ground states population ratio of the 1080 cm^{-1} vibration (b) decay lifetime, (c) transient population ratio increase, and (d) population ratio baseline of MTP (purple), CTP (orange), NBT (green), PTP (blue), and BT (gray). Each data point on (b–d) comes from one transient data set. Six data sets are taken on three different locations of one substrate for each molecule. Cross lines above the data points on (b–d) signify the statistical difference between molecules, with the *P* values acquired with *t* test. (* $P < 0.05$, ** $P < 0.01$, *** $P < 0.001$, **** $P < 0.0001$)

known that metal nanostructures are unstable with intense laser illumination, and the induced metal melting, nanoparticles aggregation, and surface reconstruction can all lead to a change in the enhancement factor of the SERS substrates.[33,34] This enhancement instability will introduce discrepancy in the ultrafast results, especially considering that the anti-Stokes and Stokes spectra are not acquired simultaneously. Therefore, we took careful precautions including using highly reproducible substrates, rotating the substrate with a spinning stage, and carefully controlling the sample illumination time as detailed in the Supporting Information.

The analytes used for this study are 4-methylbenzenethiol (MTP), 4-chlorobenzenethiol (CTP), 4-nitrobenzenethiol (NBT), biphenyl-4-thiol (PTP), and benzenethiol (BT). In Figure 2a,b, we show the anti-Stokes and Stokes spectra of the five different analytes with the paper SERS substrates. All the spectra shown here are taken with the fs pump and the ps probe temporally overlapped with each other, which is referred to as time zero. A complete set of the transient spectra (Figure 2c,d) consists of anti-Stokes and Stokes spectra taken with the pump and probe offset for different periods of time, which are also referred to as different time delays. In the Stokes spectra, multiple Raman features are present, whereas in the anti-Stokes spectra, only the peaks located around 1080 cm^{-1} are distinguishable. This is because the anti-Stokes scattering is much weaker than the Stokes scattering (*e.g.* anti-Stokes scattering is ~1% of the Stokes scattering for a 1000 cm^{-1} mode at room temperature), which means we can observe anti-Stokes features only when the vibration has a large Raman cross section or when the molecules achieve a high population in the excited vibrational state. Therefore, we carried out all the analyses with the 1080 cm^{-1} mode for all five analytes, which corresponds to the breathing mode of the phenyl ring. The similar nature of this vibrational mode in the five different analytes focuses this study on molecular specificity of energy transfer and therefore simplifies the question under study.

To quantify plasmon-induced vibrational energy transfer, we analyze the intensity of the anti-Stokes and Stokes scattering. Stokes scattering starts with molecules at the ground vibrational state, while anti-Stokes scattering starts with molecules at the first excited vibrational state. Therefore, we can obtain the excited/ground vibrational states population ratio from the relative intensity of the anti-Stokes and Stokes scattering (eq 1). The population directly reflects the vibrational energy of the monitored vibrational mode. Detailed data analysis procedure can be found in the Supporting Information.

$$\text{population ratio} = \frac{\text{intensity}_{\text{anti-Stokes}}}{C \times \text{intensity}_{\text{Stokes}}} \quad (1)$$

where the population ratio is the ratio of population at the excited and ground vibrational states, $\text{intensity}_{\text{anti-Stokes}}$ and $\text{intensity}_{\text{Stokes}}$ are the normalized anti-Stokes and Stokes scattering intensity. To normalize the intensity with wavelength-dependent SERS enhancement, we divide the peak amplitude of anti-Stokes and Stokes scattering by the extinction value at the scattering wavelength.[35] Additionally, we scale the Raman peak amplitudes with the detector efficiency at corresponding wavelength to correct for wavelength-dependent detector efficiency. In eq 1, C equals $\left(\frac{\omega_{\text{anti-Stokes}}}{\omega_{\text{Stokes}}}\right)^3$, which is a normalization factor for the wavelength dependent Raman scattering cross section. It should be noted that a cubic relationship is used here while a quadratic relationship is widely used for such analysis in previous literatures. This originates from a misinterpretation of the ω^4 dependence of Raman scattering, which can also be written as $\omega_s^3\omega_0$, with ω_s being the scattering wavelength and ω_0 being the incident wavelength. In the case of Rayleigh scattering, ω_s is equal to ω_0, so it gives the ω^4 dependence. However, for Stokes and anti-Stokes scattering, ω_0 is the same, so it reduces to a ω^3 dependence when we are taking the ratio of Stokes and anti-Stokes intensities. In older studies where intensity was

https://doi.org/10.1021/acsnano.1c08431
ACS Nano 2022, 16, 847–854

Table 1. Experimental Lifetime, Transient Population Ratio Increase and Baseline Population Ratio of Aromatic Thiols on SERS Substrate; Hammett Constant of Substituent Group, HOMO−LUMO Energy Gap (Egap) and Metal−Molecule Bond Strength (Ebond) of Aromatic Thiols/Au_{13} Cluster[36]

	4-methylbenzenethiol (MTP)	4-chlorobenzenethiol (CTP)	4-nitrobenzenethiol (NBT)	biphenyl-4-tliiol (PTP)	benzenethiol (BT)
lifetime (ps)	5.5 ± 0.6	3.3 ± 0.7	3.8 ± 0.7	3.7 ± 0.8	4.7 ± 1.0
transient Increase	0.027 ± 0.007	0.020 ± 0.005	0.010 ± 0.004	0.009 ± 0.002	0.009 ± 0.002
baseline	0.097 ± 0.006	0.05 ± 0.01	0.039 ± 0.007	0.034 ± 0.002	0.041 ± 0.003
Hammett constant	−0.17	0.23	0.78	−0.01	0
Egap (au)	0.142	0.138			0.147
Ebond (eV)	7.3	6.97			7.25

measured in the unit of energy, the correction factor with the quadratic relationship still holds true. Because E equals $\hbar\omega$, the intensity recorded in the unit of energy should be divided by $\hbar\omega$, where ω is the frequency of the scattered photons, in order to get the number of photons scattered. Notably, in this case, this correction factor C no longer purely originates from the ω^4 dependence. However, it is not applicable for modern devices which typically record in counts.

Figure 3a shows a representative example of the transient response of the excited/ground vibrational state population ratio as a function of time delay for each of the five benzenethiol derivatives. For the 1080 cm^{-1} vibration mode, the equilibrium population ratio is ∼0.0054 at room temperature without the pump or probe pulse present. All the traces have an elevated baseline population ratio (>0.0054) because the probe pulse also adds energy to molecules, and the probe is present at all time points. We refer to this population induced by the probe pulse as the baseline. At time zero, a transient population ratio increase is present, which results from the energy deposited by the pump pulse, therefore we refer to the difference between the maximum population ratio and the baseline as the transient increase. Following the increase, there is an exponential decay and the lifetime of the decay reflects how long the energy stays on the molecules after each energy deposition. By fitting the kinetic traces with an exponential decay function convoluted with the instrument response measured by the optical Kerr effect (2.0 ps), we extracted the time constant of the exponential decay and call this value the lifetime.

In Figure 3b, we show that the lifetime of the deposited vibrational energy on the 1080 cm^{-1} mode is statistically longer for MTP (5.5 ± 0.6 ps) than CTP (3.3 ± 0.7 ps), NBT (3.8 ± 0.7), PTP (3.7 ± 0.8 ps), and BT (4.7 ± 1.0 ps). In Figure 3c, we show that in terms of the transient population ratio increase, which shows the molecular response to the femtosecond pump pulse, MTP and CTP have a higher transient increase than the other molecules, although the differences between MTP and CTP or among the other three molecules are not statistically significant. In Figure 3d, we show that MTP has a significantly higher baseline, followed by CTP, then NBT and BT, while PTP is the least populated.

To investigate if the observed molecular energy trend is correlated with molecular properties, we referenced a DFT calculation study by You and co-workers,[36] where they modeled a series of para-substituent aromatic thiols on a Au_{13} cluster. With their computational results, we are able to compare molecule properties including the dipole orientation of the molecule to the metal surface, the bond strength between the metal and the molecule, the Hammett constant of the substituent group on the benzenethiol, and the HOMO−LUMO gap of the metal−molecule complex, all of which could plausibly result in the differing energy transfer efficiencies we observe experimentally.

Dipole orientation to the metal surface is an important parameter to consider when treating plasmonic−molecule systems. The coupling between molecules and the plasmonic surface, which is largely affected by the relative orientation of the molecule dipole to the metal surface normal, can have an impact on both the molecular excitation and energy decay processes.[37,38] Although the exact adsorption geometry depends on molecule surface coverage and preparation condition, previous studies have showed that the orientation of densely packed aromatic thiols are nearly upright, with a tilt angle of ∼20°−30° to the surface normal.[27−29,39] In this study, we used excessive amounts of aromatic thiols to achieve full surface coverage, so the molecules can be considered densely packed on the surface. While the surfaces used here are highly heterogeneous, the orientation of the dipole relative to the metal surface is most likely similar for the range of molecules studied due to the similarities in structure.

The metal−molecule bond strength, which directly reflects the intensity of metal−molecule interaction, is also likely to have an effect on plasmon−molecule energy transfer efficiency. Metal−molecule interactions, varying from weak physisorption to strong chemisorption, determine the extent of perturbation from the metal to the molecular orbitals and can alter the excitation mechanism of the molecules.[40] Therefore, this is an important factor to consider in plasmon-mediated catalysis and in this study.

The Hammett constant is usually used to describe the effect of a substituent group on the reactivity of benzene derivatives, which originates from the substituents' electronic influence on the connecting phenyl ring through inductive and resonance effects.[41] A previous study pointed out a strong correlation between the Hammett constant and the SERS chemical enhancement factor of a series of para-substituent benzenethiol derivatives, suggesting that there is a correlation between the substituent Hammett constant and the molecule−plasmon interaction.[42] Therefore, it is reasonable to postulate that a dependence of energy transfer on Hammett constant might be observed.

The HOMO−LUMO energy gap of the molecule is another factor which could be relevant to the molecular vibrational energy increase. When there is an overlap between molecule transition energy and the plasmon energy, a direct charge transfer process or plasmon-induced resonant energy transfer could happen, which could add energy to vibrational freedom as the molecules relax from the excited state or as the charge transfer back. Both the direct charge transfer and the resonant energy transfer mechanisms have been previously proposed for plasmon-induced catalysis.[43,44] Experiment and calculation have shown that the molecular orbitals can shift when

https://doi.org/10.1021/acsnano.1c08431
ACS Nano 2022, 16, 847−854

adsorbed onto metal surface.[45] Therefore, it is important to consider the effect of hybridization when deciding if the molecular electronic transition is resonant with the plasmon energy.

However, as shown in Table 1, none of those factors show any correlation with the energy trend on the benzenethiol derivatives, which leads us to think about this molecular specificity in the perspective of energy dissipation instead of energy capture.

Molecules with extra energy equilibrate with the surrounding environment by redistributing their energy through intermolecular interactions such as hydrogen bonding, dipole−dipole interaction, $\pi-\pi$ interaction, and London dispersion. Aromatic thiols chemically adsorb to gold surfaces through the thiol group, therefore a relatively ordered monolayer could be expected on the more planar parts of the gold surface. Outside the monolayer, a solvation layer of ∼5 nm exists under the humidity values measured during the experiments (20−30%, small daily variance), according to previous STM studies.[46] Therefore, the monolayer could generally be considered as surrounded by a solvent bath. Within the monolayer itself, the dipole−dipole interactions between molecules are restricted because all molecules are anchored on gold with relatively fixed relative orientation to the surface, leaving $\pi-\pi$ interactions the dominant intermolecular interactions. Therefore, the strength of the $\pi-\pi$ interaction will very likely affect the lifetime of the vibration excited states. In other words, when there is stronger $\pi-\pi$ interaction the intermolecular energy dissipation is more efficient, the lifetime of the energy will be shorter, and the average energy will be less on the probed molecules. On the basis of this explanation, a possible hypothesis will be that with diluted coverage of molecules on the plasmonic metal surface, the intermolecular energy transfer will be less efficient due to less intermolecular interactions. However, we were unable to test this hypothesis with the ultrafast measurements due to stringent limitations on signal-to-noise ratio in ultrafast SERS measurements.

An important factor that affects $\pi-\pi$ interaction between molecules is the molecular structure. Among MTP, CTP, and BT, the size of the substituent follows $-CH_3 > -Cl > -H$, which means that the $\pi-\pi$ stacking of the phenyl ring is the most disrupted for MTP, followed by CTP and BT.[47] On the other hand, the steric effect of the $-NO_2$ group on NBT is minimized because it is in a planar structure with the phenyl ring. Finally, aromatic thiols with multiple phenyl rings are reported to pack more efficiently compared to aromatic thiols with a single phenyl ring.[28,29,48−50] Therefore, we infer that the observed energy trend could be explained by the effect of molecular structure on $\pi-\pi$ stacking. MTP with the bulky methyl group has relative low efficiency in redistributing its energy to surrounding molecules, which leads to higher energy and an extended lifetime of the deposited energy. For CTP, it has a substituent group slightly smaller in size than the methyl group, therefore CTP has lower energy and shorter energy lifetime than MTP. Interestingly, for NBT and BT, although the size of substituent groups is different, they experienced a similar extent of energy transfer, which is significantly lower compared to CTP and MTP. This could be explained by that NBT has a planar substituent group ($-NO_2$) in plane with the phenyl ring, and BT has a substituent group ($-H$) smallest in size. This result implies that a smaller dimension of the substituent group in the orientation perpendicular to the phenyl ring is more crucial for a stronger $\pi-\pi$ interaction. Finally, PTP has the lowest energy among the five different aromatic thiols. This is possibly because the closer $\pi-\pi$ stacking facilitated by the double phenyl ring of PTP, which is more favorable for energy redistribution. Thus, the intermolecular interactions between molecules on the plasmonic surface play a key role in determining the energy transfer efficiency and lifetime of deposited energy in these aromatic thiols. Interestingly, we found significant convergence in previous literature and our observation. Namely, Ro and coworkers found that in Pt-MoOx systems, higher Mo doping leads to higher TOF of the Pt-catalyzed reverse water gas-shift reaction, while the plasmon resonance and activation energy did not shift significantly with varying doping content.[51] Additionally, it has been demonstrated in multiple systems that plasmon-induced adsorbate desorption changes the reaction energetics and promote reaction rate.[40,52,53] While these investigations were on different plasmonic and chemical systems, we think the general principal is still applicable and our results might provide additional insight into previous results.

CONCLUSION

Here we have observed plasmon-induced energy transfer kinetics and efficiency across a series of five aromatic thiols using ultrafast SERS. We find that 4-methylbenzenethiol has the highest deposited energy and longest energy lifetime after plasmon excitation, while biphenyl-4-thiol is the contrary. We attribute the observed difference to the intermolecular $\pi-\pi$ interactions in that stronger intermolecular interactions facilitate faster and more efficient molecular energy dissipation. Our results have some significant implications for the plasmonic catalysis experimental design and optimization. The most surprising implication is that reactions with a high kinetic energy barrier could possibly be facilitated by reducing, rather than increasing, the surface coverage on plasmonic metal in order to localize energy on molecules. This is something that is rarely taken into consideration for the design of plasmon-catalyzed reactions, yet it should affect the choice of reaction conditions and plasmonic catalysts. For example, molecules with strong intermolecular interactions such as thiols with phenyl ring(s) form more ordered packing structures at higher temperature as revealed by previous studies. Therefore, sample pretreatments and experimental temperature should be carefully tuned to control molecule packing to favor desired reactions. Moreover, plasmonic nanostructures could also be tailored to have features with high curvature, which could disrupt the packing pattern of reactant and at the same time create strong hot spots. Overall, we have observed that the vibrational energy transfer in plasmonic−molecule systems is likely being affected by intermolecular forces. Our conclusion can be applied to the design and optimization of plasmonic catalysis in multiple aspects including the choice of reactant concentration, reaction conditions and the morphology of plasmonic nanomaterials.

EXPERIMENTAL SECTION

Sample Preparation. We synthesized gold nanoparticles following the Frens method.[54] We fabricated SERS substrates for ultrafast measurements by drop casting 250 μl of 100× concentrated gold nanoparticles solution on each 22 mmx22 mm filter paper. The detailed synthesis of gold nanoparticles and substrate fabrication are described in the Supporting Information. We drop casted 250 μl of

https://doi.org/10.1021/acsnano.1c08431
ACS Nano 2022, 16, 847−854

300 uM benzenethiol derivative solution on the as-prepared SERS substrate and let it dry at ambient condition. Additional details can be found in the Supporting Information.

Ultrafast SERS Instrumentation. We performed ultrafast SERS measurements on a home-built instrument as described in previous literature.[55] In brief, a fundamental beam of <250 fs laser pulses centered at 1035 nm with the repetition rate of 2.04 MHz was generated from a diode-pumped Yb-fiber-amplified laser (ClarkMXR Impulse). We split the fundamental beam by a 50:50 beam splitter and sent half of the fundamental beam to a spectral filter to generate the narrowband picosecond probe beam, where the beam was dispersed by a transmission grating and then focused to a slit by a cylindrical lens. We used the rest of the fundamental beam directly as the pump beam. We used a motorized delay stage (Newport XMS500) to change the path length of the pump beam, creating various time delay between the pump and probe. We collected the scattered photons in a 90° reflection geometry. We rotated the SERS substrates at 7200 rpm with a spinning stage throughout the measurements. We used a 1000 nm short pass filter for anti-Stokes scattering and a 1064 nm long pass filter for Stokes scattering measurements. We used a 1024-pixel InGaAs array (Princeton Instruments PYLON-IR 1.7) with a 600 gr/mm grating blazed at 750 nm (Princeton Instruments, 2300i) for detection.

ASSOCIATED CONTENT

Supporting Information

The Supporting Information is available free of charge at https://pubs.acs.org/doi/10.1021/acsnano.1c08431.

Detailed sample preparation and characterization, description of the ultrafast SERS instrument and experimental details, data collection and processing procedures, and additional description of the population ratio calculations (PDF)

AUTHOR INFORMATION

Corresponding Author

Renee R. Frontiera − *Department of Chemistry, University of Minnesota, Minneapolis, Minnesota 55455, United States;* orcid.org/0000-0001-8218-7574; Phone: 612-624-2501; Email: rrf@umn.edu

Author

Ziwei Yu − *Department of Chemistry, University of Minnesota, Minneapolis, Minnesota 55455, United States*

Complete contact information is available at: https://pubs.acs.org/10.1021/acsnano.1c08431

Notes

The authors declare no competing financial interest.

ACKNOWLEDGMENTS

This work was supported by Air Force Office of Scientific Research under AFOSR sward no. FA9550-15-1-0022. This work was supported partially by the MRSEC Program of the National Science Foundation under award no. DMR-2011401.

REFERENCES

(1) Gao, C.; Low, J.; Long, R.; Kong, T.; Zhu, J.; Xiong, Y. Heterogeneous Single-Atom Photocatalysts: Fundamentals and Applications. *Chem. Rev.* **2020**, *120*, 12175−12216.

(2) Li, X.; Yu, J.; Wageh, S.; Al-Ghamdi, A. A.; Xie, J. Graphene in Photocatalysis: A Review. *Small* **2016**, *12*, 6640−6696.

(3) Twilton, J.; Le, C.; Zhang, P.; Shaw, M. H.; Evans, R. W.; MacMillan, D. W. C. The Merger of Transition Metal and Photocatalysis. *Nat. Rev. Chem.* **2017**, *1*, 1−19.

(4) Xu, C.; Anusuyadevi, P. R.; Aymonier, C.; Luque, R.; Marre, S. Nanostructured Materials for Photocatalysis. *Chem. Soc. Rev.* **2019**, *48*, 3868−3902.

(5) Aslam, U.; Rao, V. G.; Chavez, S.; Linic, S. Catalytic Conversion of Solar to Chemical Energy on Plasmonic Metal Nanostructures. *Nat. Catal.* **2018**, *1*, 656−665.

(6) Wu, N. Plasmonic Metal−Semiconductor Photocatalysts and Photoelectrochemical Cells: A Review. *Nanoscale* **2018**, *10*, 2679−2696.

(7) Maier, S. A. *Plasmonics: Fundamentals and Applications*; Springer, New York, 2007.

(8) Hartland, G. V. Optical Studies of Dynamics in Noble Metal Nanostructures. *Chem. Rev.* **2011**, *111*, 3858−3887.

(9) Brooks, J. L.; Warkentin, C. L.; Saha, D.; Keller, E. L.; Frontiera, R. R. Toward a Mechanistic Understanding of Plasmon-Mediated Photocatalysis. *Nanophotonics* **2018**, *7*, 1697−1724.

(10) Liu, Z.; Hou, W.; Pavaskar, P.; Aykol, M.; Cronin, S. B. Plasmon Resonant Enhancement of Photocatalytic Water Splitting under Visible Illumination. *Nano Lett.* **2011**, *11*, 1111−1116.

(11) Zhang, X.; Li, X.; Zhang, D.; Su, N. Q.; Yang, W.; Everitt, H. O.; Liu, J. Product Selectivity in Plasmonic Photocatalysis for Carbon Dioxide Hydrogenation. *Nat. Commun.* **2017**, *8*, 1−9.

(12) Oshikiri, T.; Ueno, K.; Misawa, H. Plasmon-Induced Ammonia Synthesis through Nitrogen Photofixation with Visible Light Irradiation. *Angew. Chem.* **2014**, *126*, 9960−9963.

(13) Brooks, J. L.; Warkentin, C. L.; Chulhai, D. V.; Goodpaster, J. D.; Frontiera, R. R. Plasmon-Mediated Intramolecular Methyl Migration with Nanoscale Spatial Control. *ACS Nano* **2020**, *14*, 17194−17202.

(14) Naya, S.; Kimura, K.; Tada, H. One-Step Selective Aerobic Oxidation of Amines to Imines by Gold Nanoparticle-Loaded Rutile Titanium(IV) Oxide Plasmon Photocatalyst. *ACS Catal.* **2013**, *3*, 10−13.

(15) Zhang, X.; Ke, X.; Zhu, H. Zeolite-Supported Gold Nanoparticles for Selective Photooxidation of Aromatic Alcohols under Visible-Light Irradiation. *Chem.−Eur. J.* **2012**, *18*, 8048−8056.

(16) Huang, X.; Li, Y.; Chen, Y.; Zhou, H.; Duan, X.; Huang, Y. Plasmonic and Catalytic AuPd Nanowheels for the Efficient Conversion of Light into Chemical Energy. *Angew. Chemie Int. Ed.* **2013**, *52*, 6063−6067.

(17) Huang, X.; El-Sayed, I. H.; Qian, W.; El-Sayed, M. A. Cancer Cell Imaging and Photothermal Therapy in the Near-Infrared Region by Using Gold Nanorods. *J. Am. Chem. Soc.* **2006**, *128*, 2115−2120.

(18) Huang, T.; Xu, X.-H. N. Synthesis and Characterization of Tunable Rainbow Colored Colloidal Silver Nanoparticles Using Single-Nanoparticle Plasmonic Microscopy and Spectroscopy. *J. Mater. Chem.* **2010**, *20*, 9867−9876.

(19) Luther, J. M.; Jain, P. K.; Ewers, T.; Alivisatos, A. P. Localized Surface Plasmon Resonances Arising from Free Carriers in Doped Quantum Dots. *Nat. Mater.* **2011**, *10*, 361−366.

(20) Jensen, T. R.; Malinsky, M. D.; Haynes, C. L.; Van Duyne, R. P. Nanosphere Lithography: Tunable Localized Surface Plasmon Resonance Spectra of Silver Nanoparticles. *J. Phys. Chem. B* **2000**, *104*, 10549−10556.

(21) Mubeen, S.; Lee, J.; Singh, N.; Krämer, S.; Stucky, G. D.; Moskovits, M. An Autonomous Photosynthetic Device in Which All Charge Carriers Derive from Surface Plasmons. *Nat. Nanotechnol.* **2013**, *8*, 247−251.

(22) Li, J.; Cushing, S. K.; Meng, F.; Senty, T. R.; Bristow, A. D.; Wu, N. Plasmon-Induced Resonance Energy Transfer for Solar Energy Conversion. *Nat. Photonics* **2015**, *9*, 601−607.

(23) Mukherjee, S.; Libisch, F.; Large, N.; Neumann, O.; Brown, L. V.; Cheng, J.; Lassiter, J. B.; Carter, E. A.; Nordlander, P.; Halas, N. J. Hot Electrons Do the Impossible: Plasmon-Induced Dissociation of H_2 on Au. *Nano Lett.* **2013**, *13*, 240−247.

(24) Christopher, P.; Xin, H.; Linic, S. Visible-Light-Enhanced Catalytic Oxidation Reactions on Plasmonic Silver Nanostructures. *Nat. Chem.* **2011**, *3*, 467−472.

(25) Remacle, F.; Levine, R. D. An Electronic Time Scale in Chemistry. *Proc. Natl. Acad. Sci. U. S. A.* **2006**, *103*, 6793−6798.
(26) Spata, V.; Carter, E. A. Mechanistic Insights into Photocatalyzed Hydrogen Desorption from Palladium Surfaces Assisted by Localized Surface Plasmon Resonances. *ACS Nano* **2018**, *12* (4), 3512−3522.
(27) Wan, L.-J.; Terashima, M.; Noda, H.; Osawa, M. Molecular Orientation and Ordered Structure of Benzenethiol Adsorbed on Gold(111). *J. Phys. Chem. B* **2000**, *104*, 3563−3569.
(28) Matei, D. G.; Muzik, H.; Gölzhäuser, A.; Turchanin, A. Structural Investigation of 1,1●-Biphenyl-4-Thiol Self-Assembled Monolayers on Au(111) by Scanning Tunneling Microscopy and Low-Energy Electron Diffraction. *Langmuir* **2012**, *28*, 13905−13911.
(29) Kang, H.; Noh, J. Structural Investigation of 4-Methylbenzenethiol Self-Assembled Monolayers on Au(111) by Scanning Tunneling Microscopy. *Bull. Korean Chem. Soc.* **2014**, *35*, 1275−1276.
(30) Liu, Y.; Jiao, Y.; Luo, H.; Huang, N.; Lai, M.; Zou, K.; Yao, H. Catalyst-Controlled Regiodivergent Synthesis of 1- and 3-Thiosugars with High Stereoselectivity and Chemoselectivity. *ACS Catal.* **2021**, *11*, 5287−5293.
(31) Laudadio, G.; Barmpoutsis, E.; Schotten, C.; Struik, L.; Govaerts, S.; Browne, D. L.; Noël, T. Sulfonamide Synthesis through Electrochemical Oxidative Coupling of Amines and Thiols. *J. Am. Chem. Soc.* **2019**, *141*, 5664−5668.
(32) Jereb, M.; Hribernik, L. Conversion of Thiols into Sulfonyl Halogenides under Aerobic and Metal-Free Conditions. *Green Chem.* **2017**, *19*, 2286−2295.
(33) Link, S.; Burda, C.; Nikoobakht, B.; El-Sayed, M. A. Laser-Induced Shape Changes of Colloidal Gold Nanorods Using Femtosecond and Nanosecond Laser Pulses. *J. Phys. Chem. B* **2000**, *104*, 6152−6163.
(34) Takami, A.; Kurita, H.; Koda, S. Laser-Induced Size Reduction of Noble Metal Particles. *J. Phys. Chem. B* **1999**, *103*, 1226−1232.
(35) Dieringer, J. A.; McFarland, A. D.; Shah, N. C.; Stuart, D. A.; Whitney, A. V.; Yonzon, C. R.; Young, M. A.; Zhang, X.; Van Duyne, R. P. Introductory Lecture Surface Enhanced Raman Spectroscopy: New Materials, Concepts, Characterization Tools, and Applications. *Faraday Discuss.* **2006**, *132*, 9−26.
(36) You, T.; Liang, X.; Gao, Y.; Yin, P.; Guo, L.; Yang, S. A Computational Study on Surface-Enhanced Raman Spectroscopy of Para-Substituted Benzenethiol Derivatives Adsorbed on Gold Nanoclusters. *Spectrochim. Acta Part A Mol. Biomol. Spectrosc.* **2016**, *152*, 278−287.
(37) Eagen, C. F.; Weber, W. H. Energy Transfer from an Excited Dye Molecule to the Surface Plasmons of an Adjacent Metal. *Opt. Lett.* **1979**, *4*, 236−238.
(38) Morawitz, H.; Philpott, M. R. Coupling of an Excited Molecule to Surface Plasmons. *Phys. Rev. B* **1974**, *10*, 4863.
(39) Kang, H.; Park, T.; Choi, I.; Lee, Y.; Ito, E.; Hara, M.; Noh, J. Formation of Large Ordered Domains in Benzenethiol Self-Assembled Monolayers on Au(111) Observed by Scanning Tunneling Microscopy. *Ultramicroscopy* **2009**, *109*, 1011−1014.
(40) Kale, M. J.; Avanesian, T.; Xin, H.; Yan, J.; Christopher, P. Controlling Catalytic Selectivity on Metal Nanoparticles by Direct Photoexcitation of Adsorbate-Metal Bonds. *Nano Lett.* **2014**, *14*, 5405−5412.
(41) Hammett, L. P. The Effect of Structure upon the Reactions of Organic Compounds. Benzene Derivatives. *J. Am. Chem. Soc.* **1937**, *59*, 96−103.
(42) Trivedi, D. J.; Barrow, B.; Schatz, G. C. Understanding the Chemical Contribution to the Enhancement Mechanism in SERS: Connection with Hammett Parameters. *J. Chem. Phys.* **2020**, *153*, 124706.
(43) Rao, V. G.; Aslam, U.; Linic, S. Chemical Requirement for Extracting Energetic Charge Carriers from Plasmonic Metal Nanoparticles to Perform Electron-Transfer Reactions. *J. Am. Chem. Soc.* **2019**, *141*, 643−647.
(44) Kazuma, E.; Jung, J.; Ueba, H.; Trenary, M.; Kim, Y. Real-Space and Real-Time Observation of a Plasmon-Induced Chemical Reaction of a Single Molecule. *Science* **2018**, *360*, 521−526.
(45) Boerigter, C.; Aslam, U.; Linic, S. Mechanism of Charge Transfer from Plasmonic Nanostructures to Chemically Attached Materials. *ACS Nano* **2016**, *10*, 6108−6115.
(46) Freund, J.; Halbritter, J.; Hörber, J. K. H. How Dry Are Dried Samples? Water Adsorption Measured by STM. *Microsc. Res. Technol.* **1999**, *44*, 327−338.
(47) Belot, V.; Farran, D.; Jean, M.; Albalat, M.; Vanthuyne, N.; Roussel, C. Steric Scale of Common Substituents from Rotational Barriers of N-(o-Substituted Aryl)Thiazoline-2-Thione Atropisomers. *J. Org. Chem.* **2017**, *82*, 10188−10200.
(48) Tao, Y. T.; Wu, C. C.; Eu, J. Y.; Lin, W. L.; Wu, K. C.; Chen, C. H. Structure Evolution of Aromatic-Derivatized Thiol Monolayers on Evaporated Gold. *Langmuir* **1997**, *13*, 4018−4023.
(49) Tour, J. M.; Jones II, L.; Pearson, D. L.; Lamba, J. J. S.; Burgin, T. P.; Whitesides, G. M.; Allara, D. L.; Parikh, A. N.; Atre, S. V. Self-Assembled Monolayers and Multilayers of Conjugated Thiols,-Dithiols, and Thioacetyl-Containing Adsorbates. Understanding Attachments between Potential Molecular Wires and Gold Surfaces. *J. Am. Chem. Soc.* **1995**, *117*, 9529−9534.
(50) Dhirani, A.-A.; Zehner, R. W.; Hsung, R. P.; Guyot-Sionnest, P.; Sita, L. R. Self-Assembly of Conjugated Molecular Rods: A High-Resolution STM Study. *J. Am. Chem. Soc.* **1996**, *118*, 3319−3320.
(51) Ro, I.; Sener, C.; Stadelman, T. M.; Ball, M. R.; Venegas, J. M.; Burt, S. P.; Hermans, I.; Dumesic, J. A.; Huber, G. W. Measurement of Intrinsic Catalytic Activity of Pt Monometallic and Pt-MoOx Interfacial Sites over Visible Light Enhanced PtMoOx/SiO_2 Catalyst in Reverse Water Gas Shift Reaction. *J. Catal.* **2016**, *344*, 784−794.
(52) Robatjazi, H.; Bao, J. L.; Zhang, M.; Zhou, L.; Christopher, P.; Carter, E. A.; Nordlander, P.; Halas, N. J. Plasmon-Driven Carbon−Fluorine ($C(sp^3)$−F) Bond Activation with Mechanistic Insights into Hot-Carrier-Mediated Pathways. *Nat. Catal.* **2020**, *3*, 564−573.
(53) Zhou, L.; Swearer, D. F.; Zhang, C.; Robatjazi, H.; Zhao, H.; Henderson, L.; Dong, L.; Christopher, P.; Carter, E. A.; Nordlander, P.; Halas, N. J. Quantifying Hot Carrier and Thermal Contributions in Plasmonic Photocatalysis. *Science* **2018**, *362*, 69−72.
(54) Frens, G. Controlled Nucleation for the Regulation of the Particle Size in Monodisperse Gold Suspensions. *Nat. Phys. Sci.* **1973**, *241*, 20−22.
(55) Keller, E. L.; Frontiera, R. R. Ultrafast Nanoscale Raman Thermometry Proves Heating Is Not a Primary Mechanism for Plasmon-Driven Photocatalysis. *ACS Nano* **2018**, *12*, 5848−5855.

https://doi.org/10.1021/acsnano.1c08431
ACS Nano 2022, 16, 847−854